Observation of Entanglement-Dependent Two-Particle Holonomic Phase

J. C. Loredo,* M. A. Broome, D. H. Smith, and A. G. White
Centre for Engineered Quantum Systems, Centre for Quantum Computer and Communication Technology, and School of Mathematics and Physics, University of Queensland, Brisbane, Queensland 4072, Australia
(Received 6 November 2013; published 10 April 2014)

Holonomic phases—geometric and topological—have long been an intriguing aspect of physics. They are ubiquitous, ranging from observations in particle physics to applications in fault tolerant quantum computing. However, their exploration in particles sharing genuine quantum correlations lacks in observations. Here, we experimentally demonstrate the holonomic phase of two entangled photons evolving locally, which, nevertheless, gives rise to an entanglement-dependent phase. We observe its transition from geometric to topological as the entanglement between the particles is tuned from zero to maximal, and find this phase to behave more resiliently to evolution changes with increasing entanglement. Furthermore, we theoretically show that holonomic phases can directly quantify the amount of quantum correlations between the two particles. Our results open up a new avenue for observations of holonomic phenomena in multiparticle entangled quantum systems.

DOI: 10.1103/PhysRevLett.112.143603 PACS numbers: 42.50.-p, 03.65.Vf

In differential geometry, holonomy accounts for the difference between a parallel-transported vector along a geodesic—i.e., shortest path—and any other curve. It is a direct manifestation of the geometry and topology of a given curved space. A physical system evolving in its own multidimensional parameter space will exhibit holonomies as a result of these geometric and topological structures. Consequently, holonomies have physical manifestations, ranging from Thomas precession to the Aharonov-Bohm effect.

In quantum systems, the holonomy manifests as a phase imparted on the wave function [1]. When the quantum parameter space is simply connected, holonomies are continuous valued with respect to continuous deformations of the trajectory. These are geometric phases [2], and they depend on the space's curvature. Conversely, when the parameter space is not simply connected, discrete-valued topological phases appear [3,4]. We refer to both geometric and topological as holonomic phases.

Holonomies are of fundamental interest and have important applications, for example, in holonomic quantum computation [5–8], where matrix-valued geometric phase transformations play the role of quantum logic gates. This scheme has received a great deal of attention due to its potential to overcome decoherence [9], and has recently been experimentally realized in different architectures [10,11].

In the quantum regime, holonomic phases have been observed in particles encoding one qubit [12–14], as well as two particle systems encoding uncorrelated two-qubit states [15]. In addition, topological phases have been observed in classical systems emulating the behavior of entanglement, for example, so-called nonseparable states between the polarization and transverse modes of a laser [16], or pseudoentanglement in NMR [17]. Lacking up to now, however, is the exploration of holonomic phases between genuinely entangled quantum particles.

Here, we demonstrate both geometric and topological phases appearing in the joint wave function of two separate, and genuinely entangled, particles whose correlations can be tuned from vanishing to maximal.

To better elucidate two-qubit holonomic phases, consider an arbitrary two-qubit pure state written in its Schmidt decomposition

$$|\psi(0)\rangle = e^{-i\beta/2}\cos\frac{\alpha}{2}|n_a m_b\rangle + e^{i\beta/2}\sin\frac{\alpha}{2}|n_a^{\perp} m_b^{\perp}\rangle, \quad (1)$$

where $\alpha \in [0,\pi]$ and $\beta \in [0,2\pi]$ parametrize the Schmidt sphere [18] of a correlation space, and $|n_a m_b\rangle$, $|n_a^{\perp} m_b^{\perp}\rangle$ are orthogonal product states defining the Schmidt basis, see Figs. 1(a) and 1(b). While a treatment of the two-qubit space can be carried out formally [19], it is more intuitive to represent evolutions in it with the trajectories that the reduced density matrices, ρ_a and ρ_b, undertake on their corresponding local Bloch spheres together with the curve that α and β project onto the Schmidt sphere.

For a nonmaximally entangled state, $|\psi(0)\rangle$ has preferred directions, given by unit vectors $\hat{a}$ and $\hat{b}$, on each qubit's Bloch sphere. That is, the reduced density matrix of, say, system a is given by $\rho_a = \mathrm{Tr}_b(|\psi\rangle\langle\psi|) = (1/2)(\mathbb{I} + \cos\alpha\hat{a}\cdot\vec{\sigma})$, where $\vec{\sigma} = (\sigma_x, \sigma_y, \sigma_z)$ denote the Pauli matrices. Accordingly, $|\psi(0)\rangle$ spans a six-dimensional parameter space.

From the state $|\psi(0)\rangle$, an entanglement-induced holonomic phase will appear as a result of the special "Schmidt evolution." We define a Schmidt evolution as a bilocal rotation of θ_S, of both qubits around their preferential directions $\hat{a}$ and $\hat{b}$, see Fig. 1(a). The holonomic phase of this evolution is calculated—in the standard way—as a difference [20]

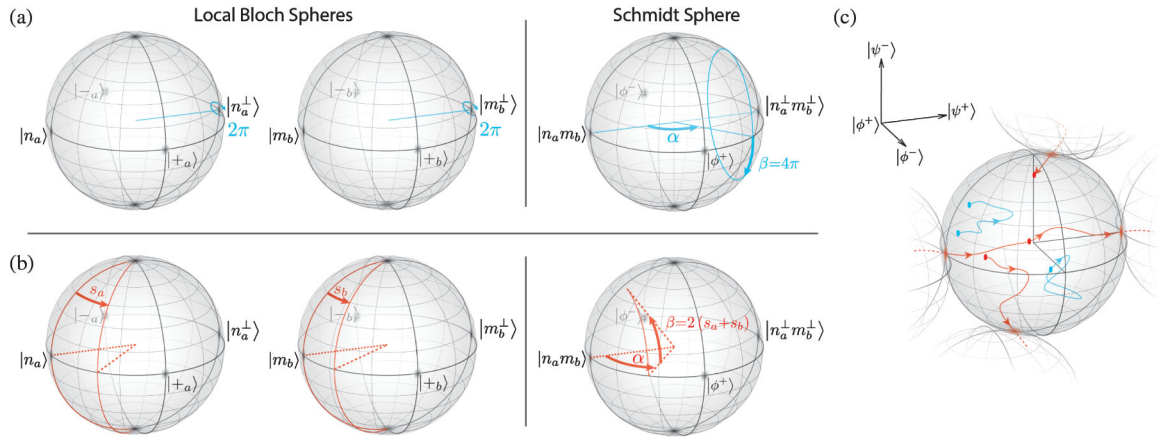

FIG. 1 (color). (a) A cyclic Schmidt evolution with $\theta_S = 2\pi$. Left and middle spheres show trajectories traced out in the local Bloch spheres of each qubit defined in the Schmidt basis. Here, they evolve at a single point and, therefore, enclose no area, leading to no gain in holonomic phase. The right sphere represents the trajectory spanned by the evolution of α and β in the Schmidt sphere. In contrast to the local trajectories, a holonomic phase still arises as a result of the area enclosed by this trajectory. Equivalent Schmidt evolutions of nonentangled states induce a zero holonomic phase. (b) In contrast, segmented evolutions defined by angles s_a and s_b induce holonomies appearing from both local and Schmidt spheres. The parameters s_a and s_b define the opening angles for the projected curves of ρ_a and ρ_b onto the local Bloch spheres. In the right sphere, a rotation angle $2(s_a + s_b) = \beta$ around $|n_a m_b\rangle$ also contributes to the holonomy. Equivalent evolutions of nonentangled states induce a nonzero holonomic phase. (c) Depiction of the double-connected parameter space of maximally entangled states: SO(3) in $\mathbb{R}^3$ with a border at S^2_π. This border is a two sphere of radius π with identified antipodal points. Blue trajectories represent arbitrary evolutions for one homotopy class along which no phase is gained. Red curves represent evolutions of the other homotopy class after which a π phase appears on the wave function.

$$\Phi_h = \Phi_P - \Phi_{\mathrm{dyn}}, \tag{2}$$

with $\Phi_P = \arg\langle\psi(0)|\psi(\tau)\rangle$ the Pancharatnam [21] and $\Phi_{\mathrm{dyn}} = \mathrm{Im}\int_0^\tau \langle\psi(t)|\dot{\psi}(t)\rangle dt$ the dynamical phase, and $|\psi(t)\rangle$, $t \in [0, \tau]$, denotes the evolving state.

While, usually, Φ_h is regarded as a geometric phase only [20], its value arises from both the geometry (curvature) and topology (connectedness) of the parameter space. Therefore, it has become more routine to identify parts of Φ_h as being of either geometric or topological origin [22]. For instance, maximally entangled two-qubit pure states (MESs) can only induce a phase of topological origin regardless of their evolution [3,4,22].

Canonically, the amount of entanglement in a two-qubit state can be measured by the tangle $\mathbb{T}$ (concurrence squared [23]). In a pure system as given in Eq. (1), it is determined by the relative populations of the Schmidt basis: $\mathbb{T} = \sin^2\alpha$, and ranges from 0 for separable states up to 1 for maximally entangled states. Consequently, a Schmidt evolution will give rise to, see Supplemental Material [24], an entanglement-induced holonomic phase given by

$$\Phi_h^{\mathrm{ent}} = \arg\left(\cos\theta_S - i\sqrt{1-\mathbb{T}}\sin\theta_S\right) + \theta_S\sqrt{1-\mathbb{T}}. \tag{3}$$

Importantly, Φ_h^{ent} behaves monotonically with the amount of entanglement, measuring 0 for separable states and its maximum for MESs (value depended on θ_S). For instance, for the evolution depicted in Fig. 1(a), $\theta_S = 2\pi$, and $\Phi_h^{\mathrm{ent}} = -2\pi(1-\sqrt{1-\mathbb{T}})$. While there are extensive theoretical studies of holonomic phases in mixed, as well as pure, entangled systems [25–27], it remains an open question as to whether a holonomic phase quantifying entanglement can be found for mixed states.

Recalling that, experimentally, it is the total Pancharatnam phase that is observed [28], we can choose evolutions for which the dynamical component vanishes, ensuring the total phase gained is holonomic in nature only. We achieve this using the bilocal segmented evolutions characterized by the opening angles s_a and s_b on qubits a and b, respectively, see Fig. 1(b). These trajectories are connected geodesics, meaning any dynamical phase is identically zero. However, not being Schmidt evolutions, the holonomic phase arises from trajectories in both local and Schmidt spheres, but, importantly, remains monotonic with entanglement

$$\Phi_h = \mp \arctan\left(\sqrt{1-\mathbb{T}}\tan(2s)\right), \tag{4}$$

where the sign is $-$ $(+)$ if the joint state is more populated in $|n_a m_b\rangle$ $(|n_a^\perp m_b^\perp\rangle)$ of the Schmidt basis, see Supplemental Material [24], and s defines the evolution undertaken by $|\psi(0)\rangle$. In Eq. (4), the opening angles $s_a = s_b = s$.

One important feature of the state in Eq. (1) is the change that occurs to the parameter space as a result of increasing tangle. As $\mathbb{T} \to 1$, previously separated states in the two-qubit parameter space become less distinguishable, and

eventually some become identical at $\mathbb{T} = 1$. At this point, the parameter space collapses from six to three dimensions represented by the double-connected SO(3) ball [3,4], see Fig. 1(c). Spaces of this kind—not simply connected—allow state trajectories that are topologically distinct, i.e., cannot be continuously transformed into one another.

Trajectories in the SO(3) ball are classified by two different homotopy-class families: those that cross the border S^2_π—a two sphere of radius π—an odd number of times and those crossing it an even number of times (zero included). Physically, crossing S^2_π l times results in a $l\pi$ phase on the wave function. For instance, if $\alpha = \pi/2$ in the Schmidt evolution shown in Fig. 1(a), then its trajectory in SO(3) crosses S^2_π twice, picking up a 2π topological phase.

In order to observe the entanglement-dependent holonomic phase given by Eq. (4), we implement a method, depicted in Fig. 2, that works as follows: We generate a two-qubit state, $|\psi\rangle$, in the polarization of two single photons whose tangle can be tuned from $\mathbb{T} = 0 \to 1$ [29,30]. Upon meeting at the first 50:50 beam splitter BS1 of the interferometer depicted in Fig. 2(a), the photons are subject to nonclassical interference [31], after which they exit via the same spatial mode. Regardless of the specific form of $|\psi\rangle$, photon bunching can always be achieved by engineering other degrees of freedom if necessary [32]. Consequently, the joint state of the system, $|\psi\rangle$, remains in either of the two paths of the interferometer, whose optical path lengths are equal. The joint state then undergoes a polarization evolution, composed of two auxiliary evolutions $\check{U}$ and $\hat{U}$ in separate paths of the interferometer.

The information about which path the photons followed is erased by a second 50:50 beam splitter BS2, after which point the photons are detected. As such, the two-photon coincidence signal, c, will exhibit interference behavior modulated by all relative phases between the two arms of the interferometer. That is, caused by a physical optical path-difference phase ϕ and the Pancharatnam phase Φ_P arising from the polarization evolutions.

We prepared the initial polarization-entangled state $|\psi\rangle = \cos(\alpha/2)|HH\rangle + \sin(\alpha/2)|VV\rangle$, where α is a tuneable parameter defining the amount of entanglement $\mathbb{T} = \sin^2\alpha$, and $|H\rangle$ and $|V\rangle$ denote the horizontal and vertical polarizations. The state is injected into a displaced-Sagnac interferometer configuration, shown in Fig. 2(b), where no active path locking is required. Using the notation $\sigma_1 = |H\rangle\langle H| - |V\rangle\langle V|$ and $\sigma_2 = |H\rangle\langle V| + |V\rangle\langle H|$, we choose an evolution

$$U \equiv \hat{U}^\dagger \check{U} = e^{i(\pi/4)\sigma_2} e^{-i(\pi/2)(\sigma_1 \sin s + \sigma_2 \cos s)} e^{i(\pi/4)\sigma_2}, \quad (5)$$

where s equals the opening angles of the corresponding geodesic trajectories in the local spaces, see Fig. 1(b). Since the evolutions $\check{U}$ and $\hat{U}$ are chosen to induce no dynamical phase, from Eq. (2), the Pancharatnam phase matches the holonomic phase. Thus, by controlling the variable phase ϕ—introduced by slightly rotating the mirror $M3$ of the interferometer, see Fig. 2(b)—the two-photon coincidence will modulate as

$$\begin{aligned} c &= \frac{1}{4}|e^{2i\phi}|\psi\rangle + (\hat{U}^\dagger \check{U} \otimes \hat{U}^\dagger \check{U})|\psi\rangle|^2 \\ &= \frac{1}{2}[1 + v\cos(2\phi - \Phi_h)], \end{aligned} \quad (6)$$

where $v = |\langle\psi|\psi'\rangle|$ is the interference visibility and $\Phi_h = \arg\langle\psi|\psi'\rangle$ is the holonomic phase gained during the effective evolution $|\psi'\rangle = U \otimes U|\psi\rangle$. Consequently, we can determine Φ_h by measuring coincidence modulation as a function of ϕ, see Supplemental Material [24].

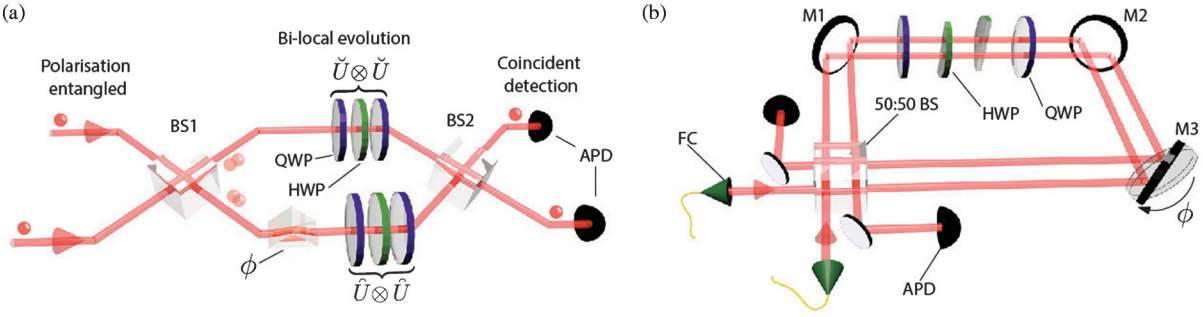

FIG. 2 (color). (a) Depiction of the experimental method. Two indistinguishable photons, encoding a two-qubit entangled state $|\psi\rangle$ in their polarization, pass through an interferometer and are detected in coincidence with avalanche-photo-diodes (APD) at the output. Because of the Hong-Ou-Mandel effect at the first beam splitter BS1, a coincidence signal c after the exit of the interferometer through BS2, cannot distinguish between different paths travelled in the interferometer. The resulting holonomic phase gained by the evolved state $|\psi'\rangle = \hat{U}^\dagger \check{U} \otimes \hat{U}^\dagger \check{U}|\psi\rangle$, as well as the phase ϕ, thus, appears as a modulation in the coincidence given by $c \propto |e^{2i\phi}|\psi\rangle + |\psi'\rangle|^2$. (b) Experimental implementation of the method. Single photons are injected via single-mode fiber couplers (FC) into a displaced-Sagnac interferometer configuration, composed of one 50:50 beam splitter (BS) and three mirrors $M1$–$M3$. Polarization evolution is performed using two common-path quarter wave plates QWP and two semicircular half wave plates HWP in separate optical paths. Mirror $M3$ is rotated via a microtranslation stage to control ϕ.

The polarization evolution in Eq. (5) is implemented using quarter Q and half wave plates H in the arrangement $U = Q(-\pi/4)H((\pi/4) - (s/2))Q(-\pi/4)$, where the arguments inside parentheses indicate the angle of the wave-plate optic axis in the laboratory frame. This unitary evolution is built from auxiliaries in separate arms of the interferometer, given by $\check{U} = Q(-\pi/4)H((\pi/4) - (s/4))Q(-\pi/4)$ and $\hat{U} = Q(\pi/4)H(-(\pi/4) - (s/4))Q(\pi/4)$. Physically, we perform these evolutions using two common-path quarter wave plates with angles fixed at $-(\pi/4)$ and two semicircular half wave plates, one in each path, see Fig. 2(b).

Figure 3(a) shows our predicted and measured results for Φ_h, as a function of entanglement represented by α, and the opening angle s of the trajectories. The solid and dashed black lines in Fig. 3(b) show theoretical predictions for the bipartite holonomic phase for a fitted value of tangle, $\mathbb{T} = 0.01 \pm 0.01$. In this case, the holonomy is simply the sum of individual geometric phases $\Phi_h^{\text{sep}} = \mp(s + s)$.

Conversely, as the amount of entanglement increases to a maximum, i.e., as $\alpha \to \pi/2$, the holonomic phase becomes less affected by changes in the trajectory angle s. Instead, two attractors at $\Phi_h = 0$ and $\Phi_h = \pi$ appear, becoming its only possible values when $\mathbb{T} = 1$, shown by the solid red curves in Fig. 3(b). Thus, the tuning from $\alpha = 0 \to \alpha = \pi/2$ results in a geometric-to-topological transition of the holonomic phase. The solid and dashed blue curves in Fig. 3(b) show our measurements for the fitted value of tangle, $\mathbb{T} = 0.99 \pm 0.01$.

This reported tangle is the best-fitted value to our data using Eq. (4). To confirm the presence of a high amount of entanglement, we carried out a full quantum state tomography of the two-photon state, resulting in a tangle of $\mathbb{T}_{\text{tomo}} = 0.959 \pm 0.001$, see Supplemental Material [24].

As discussed previously, when $\mathbb{T} = 1$, the corresponding evolutions follow trajectories in the double-connected SO(3) space, thus, giving rise to two topologically distinct paths. Figure 3(c) shows the corresponding paths for five such evolutions, for which the trajectory with $s = \pi/4$ represents the switch between two of the distinct homotopy classes.

Experiments [16,17] observing such topological phases have been realized with cyclic evolutions using classical states that are formally equivalent to a MES, corresponding to the top and bottom data points at $\alpha = \pi/2$ in Fig. 3(a). In contrast, we additionally demonstrated topological behavior for explicitly noncyclic evolutions, see Fig. 3(c), of genuinely entangled quantum systems.

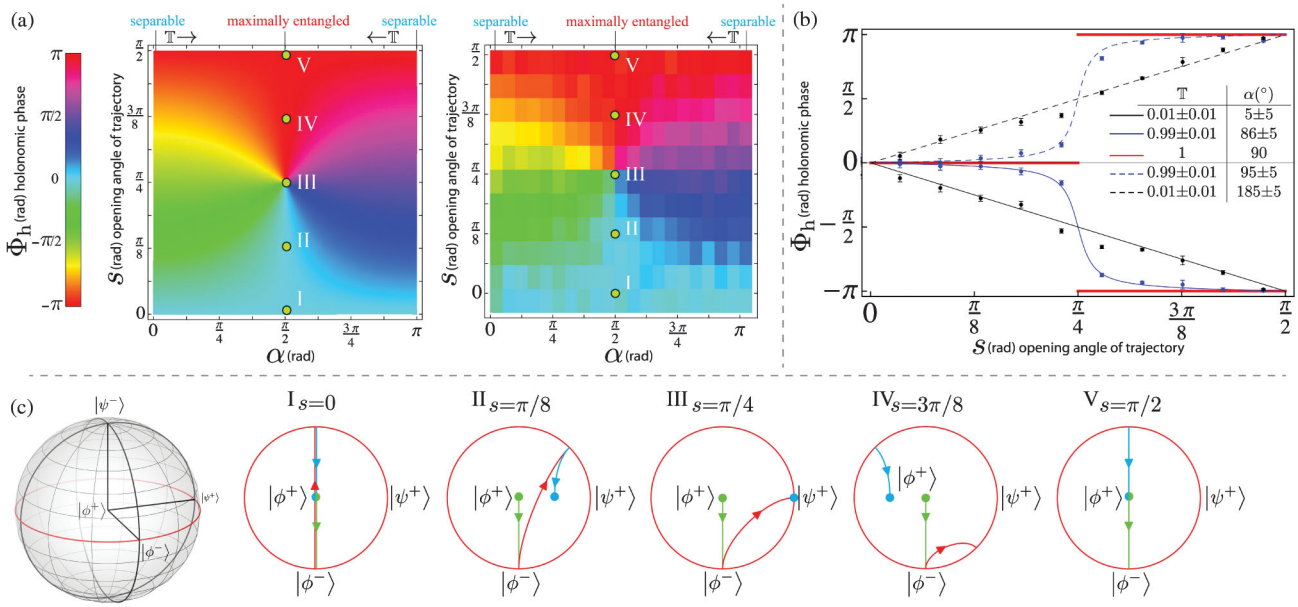

FIG. 3 (color). Experimental results. (a) In a cyclic color scale, predicted (left) and measured (right) results for $\Phi_h = -\arctan[\cos(\alpha)\tan(2s)]$ [equivalent to Eq. (4)]. Centers of the rectangular measured data blocks represent the corresponding (α, s) coordinates. (b) The black data points and theoretical curves correspond to measurements of holonomic phases with an initial state $|HH\rangle$ (solid curve) and $|VV\rangle$ (dashed curve) for a fitted level of tangle, $\mathbb{T} = 0.01 \pm 0.01$. Blue data points and theoretical curves show the extent to which we observe the topological behavior of Φ_h for a highly entangled state. Here, the data are fitted to a state tangle of $\mathbb{T} = 0.99 \pm 0.01$, for the cases in which $|\psi(0)\rangle$ is more populated by $|HH\rangle$ ($\alpha = \pi/2 - \epsilon$) shown by the solid curve, and $|VV\rangle$ ($\alpha = \pi/2 + \epsilon$) given by the dashed curve, for $0 < \epsilon \ll 1$. The red curve corresponds to the theoretical ideal case of $\mathbb{T} = 1$. Errors are calculated via Poissonian counting statistics. (c) Depiction of cyclic (I,V) and noncyclic (II,III,IV) evolutions of MESs in a plane of the double-connected SO(3) ball. Green, red, and blue colored curves denote the first, second, and third parts of each evolution, respectively. Evolution III for which $s = \pi/4$, marks the switch between two distinct homotopy classes, those that cross the S_π^2 border zero times (I and II) and one time (IV and V).

We experimentally demonstrated that the wave function of a pair of qubits picks up a phase factor of holonomic nature in both cyclic and noncyclic evolutions. In contrast to conventional measurements of single-qubit holonomic phases [12,13], the phase shift observed in our Letter is dependent on genuine quantum correlations. We find that the holonomic phase becomes more resilient to evolution changes with increasing entanglement, which indicates that quantum correlations can be utilized to enhance holonomic robustness, and there may be advantages in using not only geometric, but also the full range of holonomic phases. Naturally, this leads to the question whether more general forms of quantum correlations—most notably discord [33]—could be the underlying reason for this enhancement.

Finally, we derived an entanglement-induced holonomic phase that can be used to quantify the amount of quantum correlations between a pair of pure-state qubits. This result provides a measurable quantity arising solely from entanglement and it is a step in gaining a broader understanding of the geometric interpretation of quantum correlations. We expect that this Letter will strongly motivate new proposals for more robust holonomic quantum computation and trigger observations of holonomies in multipartite entangled states of qubits or higher-dimensional qudit systems.

We thank G. J. Milburn for stimulating discussions, and A. Fedrizzi, C. Branciard, I. Kassal, and M. Ringbauer for critical feedback. This work was supported by: the ARC Centre for Quantum Computation and Communication Technology (Grant No. CE110001027), the Centre for Engineered Quantum Systems (Grant No. CE110001013), and the Federation Fellow Program (Grant No. FF0668810).

*juan.loredo1@gmail.com

[1] B. Simon, Phys. Rev. Lett. **51**, 2167 (1983).
[2] M. V. Berry, Proc. R. Soc. A **392**, 45 (1984).
[3] P. Milman and R. Mosseri, Phys. Rev. Lett. **90**, 230403 (2003).
[4] W. LiMing, Z. L. Tang, and C. J. Liao, Phys. Rev. A **69**, 064301 (2004).
[5] P. Zanardi and M. Rasetti, Phys. Lett. A **264**, 94 (1999).
[6] L.-M. Duan, J. I. Cirac, and P. Zoller, Science **292**, 1695 (2001).
[7] L.-A. Wu, P. Zanardi, and D. A. Lidar, Phys. Rev. Lett. **95**, 130501 (2005).
[8] E. Sjöqvist, D. M. Tong, L. M. Andersson, B. Hessmo, M. Johansson, and K. Singh, New J. Phys. **14**, 103035 (2012).
[9] S. Filipp, J. Klepp, Y. Hasegawa, C. Plonka-Spehr, U. Schmidt, P. Geltenbort, and H. Rauch, Phys. Rev. Lett. **102**, 030404 (2009).
[10] A. A. Abdumalikov, Jr, J. M. Fink, K. Juliusson, M. Pechal, S. Berger, A. Wallraff, and S. Filipp, Nature (London) **496**, 482 (2013).
[11] G. Feng, G. Xu, and G. Long, Phys. Rev. Lett. **110**, 190501 (2013).
[12] P. G. Kwiat and R. Y. Chiao, Phys. Rev. Lett. **66**, 588 (1991).
[13] M. Ericsson, D. Achilles, J. T. Barreiro, D. Branning, N. A. Peters, and P. G. Kwiat, Phys. Rev. Lett. **94**, 050401 (2005).
[14] F. M. Cucchietti, J.-F. Zhang, F. C. Lombardo, P. I. Villar, and R. Laflamme, Phys. Rev. Lett. **105**, 240406 (2010).
[15] H. Kobayashi, Y. Ikeda, S. Tamate, T. Nakanishi, and M. Kitano, Phys. Rev. A **83**, 063808 (2011).
[16] C. E. R. Souza, J. A. O. Huguenin, P. Milman, and A. Z. Khoury, Phys. Rev. Lett. **99**, 160401 (2007).
[17] J. Du, J. Zhu, M. Shi, X. Peng, and D. Suter, Phys. Rev. A **76**, 042121 (2007).
[18] E. Sjöqvist, Phys. Rev. A **62**, 022109 (2000).
[19] L. Jakóbczyk and M. Siennicki, Phys. Lett. A **286**, 383 (2001).
[20] N. Mukunda and R. Simon, Ann. Phys. **228**, 205 (1993).
[21] S. Pancharatnam, Proc. Indian Acad. Sci. A **44**, 247 (1956).
[22] P. Milman, Phys. Rev. A **73**, 062118 (2006).
[23] S. Hill and W. K. Wootters, Phys. Rev. Lett. **78**, 5022 (1997).
[24] See Supplemental Material at http://link.aps.org/supplemental/10.1103/PhysRevLett.112.143603 for derivation of the holonomic phases presented in the Letter, data of the observed coincidence signal, a comparison to the case of fully-distinguishable photons, and state tomography data.
[25] D. M. Tong, E. Sjöqvist, L. C. Kwek, C. H. Oh, and M. Ericsson, Phys. Rev. A **68**, 022106 (2003).
[26] M. Ericsson, A. K. Pati, E. Sjöqvist, J. Brännlund, and D. K. L. Oi, Phys. Rev. Lett. **91**, 090405 (2003).
[27] M. Johansson, M. Ericsson, K. Singh, E. Sjöqvist, and M. S. Williamson, Phys. Rev. A **85**, 032112 (2012).
[28] J. C. Loredo, O. Ortíz, R. Weingärtner, and F. De Zela, Phys. Rev. A **80**, 012113 (2009).
[29] A. Brańczyk, A. Fedrizzi, T. Stace, T. Ralph, and A. White, Opt. Express **19**, 55 (2011).
[30] D. H. Smith, G. Gillett, M. P. de Almeida, C. Branciard, A. Fedrizzi, T. J. Weinhold, A. Lita, B. Calkins, T. Gerrits, H. M. Wiseman *et al.*, Nat. Commun. **3**, 625 (2012).
[31] C. K. Hong, Z. Y. Ou, and L. Mandel, Phys. Rev. Lett. **59**, 2044 (1987).
[32] S. P. Walborn, A. N. de Oliveira, S. Pádua, and C. H. Monken, Phys. Rev. Lett. **90**, 143601 (2003).
[33] H. Ollivier and W. H. Zurek, Phys. Rev. Lett. **88**, 017901 (2002).